Electronic Supplementary Material (ESI) for Materials Advances.

Electronic Supplementary Information for:

Morphological and Mechanical Characterization of High-Strength Sulfur Composites Prepared with Variably-Sized Lignocellulose Particles

Moira K. Lauer,[a] Zoe E. Sanders,[b] Ashlyn D. Smith [a,b] and Rhett C. Smith [a]*

[a.]Department of Chemistry, Clemson University, Clemson, South Carolina, 29634, USA.
[b]Department of Chemistry and Biology, Anderson University, Anderson, South Carolina, 29621, USA.

1. Instrumentation

Fourier transform infrared spectra were obtained using an IR instrument (Shimadzu IRAffinity-1S) with an ATR attachment. Scans were collected over the range 400–4000 cm^{-1} at ambient temperature with a resolution of 8. TGA was recorded (Mettler Toledo TGA 2 STARe System) over the range 20–800 °C with a heating rate of 10 °C·min^{-1} under a flow of N_2 (100 mL·min^{-1}). Each measurement was acquired in duplicate and presented results represent an average value. DSC was acquired (Mettler Toledo DSC 3 STARe System) over the range −60 to 150 °C with a heating rate of 5 °C·min^{-1} under a flow of N_2 (200 mL·min^{-1}). Each DSC measurement was carried out over three heat-cool cycles. Each measurement was acquired in duplicate to ensure consistent results were obtained. Carbon disulfide extractions were performed by suspending 0.3 g of finely ground material (measured to 0.0001 g) in 20 mL of CS_2, allowing the solid to settle for 30 minutes, pipetting off the supernatant into a separate vial, and adding another 20 mL of CS_2. This process was repeated an additional 3 times so that a total of 5 washes was performed. The residual CS_2 was evaporated under a flow of N_2 and each vial was weighed to determine the fraction that was soluble (collected as supernatant) or insoluble (remained in the initial vial). Compressional analysis was performed on a Mark-10 ES30 test stand equipped with a M3-200 force gauge (1 kN maximum force with ±1 N resolution). Compression cylinders were cast from silicone resin moulds (Smooth-On Oomoo® 30 tin-cure) with diameters of approximately 6 mm and heights of approximately 10 mm. Samples were manually sanded to ensure uniform dimensions and measured with a digital calliper with ±0.01 mm resolution. Compressional analysis was performed at least in triplicate and results were averaged. SEM and EDS were acquired on a Schottky Field Emission Scanning Electron Microscope SU5000 operating in variable pressure mode with an accelerating voltage of 15 keV.

2. Peanut Shell Fractionation

Peanut shells were fractionated manually using ASTM graded sieves. This process began with drying peanut shell powder in a 40 °C oven for 4 hours at 70 mmHg of reduced pressure. The peanut shells were then passed through the largest sieve to retain pieces of shell that were 710 μm. The few small pieces of this size were thrown away. The powder was then passed through a sieve with a 500 μm cut-off. The retained shells were again sieved with the largest sieve (710 μm) cut-off as well as the second largest sieve (500 μm) to ensure optimal fractionation. This process was continued to generate a total of 8 fractions of peanut shells named PS-X (where X is an integer denoting the order of collection) with sizes correlating to **Table S1**.

Table S1. Peanut shell fractionation codes and size cutoffs.

Fraction code	Minimum size cutoff	Maximum size cutoff
PS-1	500	710
PS-2	300	500
PS-3	250	300
PS-4	212	250
PS-5	150	212
PS-6	125	150
PS-7	75	125
PS-8	0	75

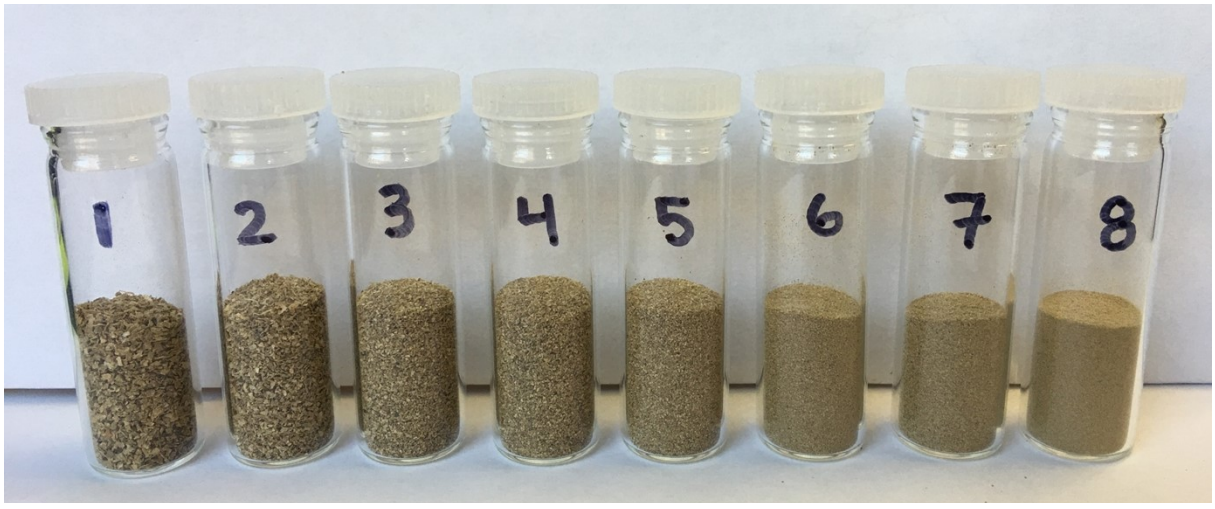

Figure S1. Digital image of peanut shell fractions in order of largest (**PS-1**) to smallest (**PS-8**).

3. Synthesis of PSS-X

Peanut shells and sulfur in a 1:9 ratio were mixed well and placed in a 20 mL scintillation vial with a Teflon coated stir bar. The vial was capped and vented with a needle to allow the moisture produced from the peanut shells to escape. The reactions were placed in a 180 °C oil bath and allowed to continue until all samples became visible homogeneous. The molten material was then poured into silicone molds for compressional analysis.

PSS-1 and PSS-2

These two samples, although homogeneous with stirring, exhibited significant separation when trying to pour the samples into molds because of the relatively high density of the large chunks of shell. Significant phase separation was also observed after cooling of the material. Because consistent sample preparation was not feasible, these two samples were omitted from analysis.

PSS-3–8

The remaining samples were all able to be poured and did not experience phase separation after cooling at room temperature for several days. The reaction conditions are summarized in **Table S2**. Target ratios were 1 part peanut shell to 9 parts sulfur, considering each peanut shell sample exhibited a moisture of ~10% (by duplicate TGA analysis).

Table S2. Synthesis conditions for **PSS-1–8**

material code	sulfur	peanut shells
PSS-1	9.001	1.102
PSS-2	9.002	1.103
PSS-3	9.001	1.100
PSS-4	9.002	1.103
PSS-5	9.001	1.102
PSS-6	9.002	1.103
PSS-7	9.000	1.101
PSS-8	9.002	1.103

4. DSC of PS-3

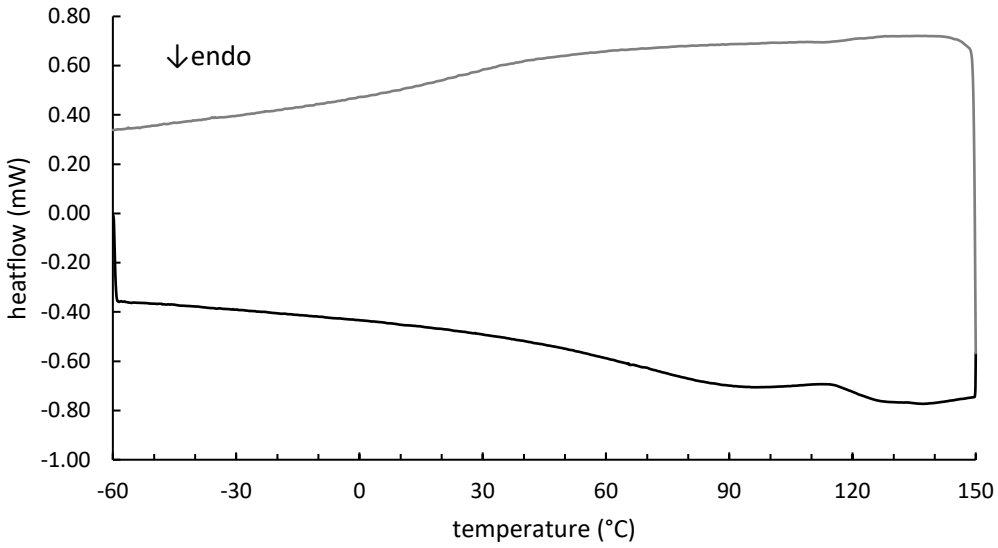

Figure S2. DSC heating (black) and cooling (gray) curves for **PS-3** from the third cycle. The third cycle was identical to the second cycle. The first cycle was obstructed by the desorption of moisture. The heating cycle exhibited a broad and convoluted T_g characteristic of cellulose from ~30–90 °C and two overlapping glass transitions with a midpoint of 124 °C. The cooling cycle showed similar transitions on cooling.

5. DSC of PS-4

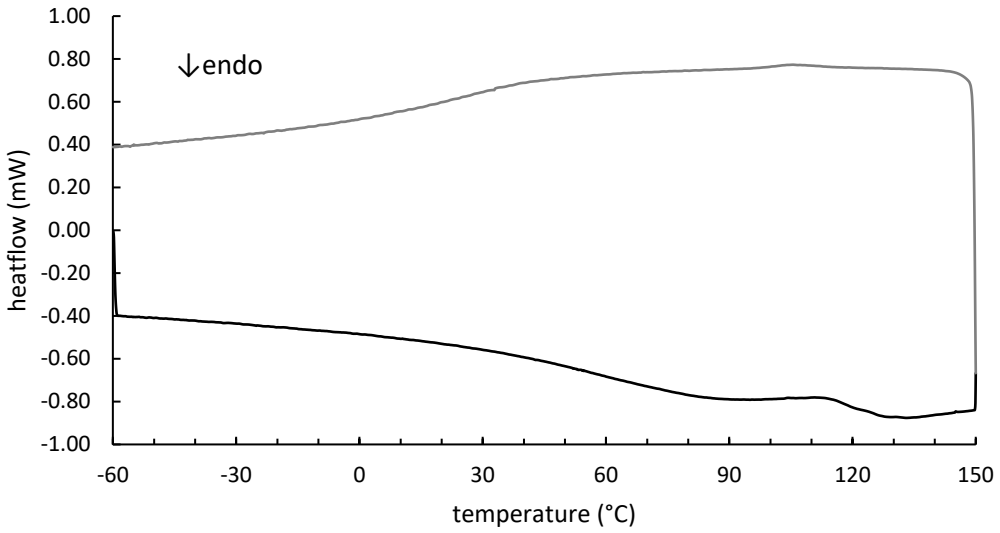

Figure S3. DSC heating (black) and cooling (gray) curves for **PS-4** from the third cycle. The third cycle was identical to the second cycle. The first cycle was obstructed by the desorption of moisture. The heating cycle exhibited a broad and convoluted T_g characteristic of cellulose from ~30–90 °C and two overlapping glass transitions with a midpoint of 123 °C. The cooling cycle showed similar transitions on cooling.

6. DSC of PS-5

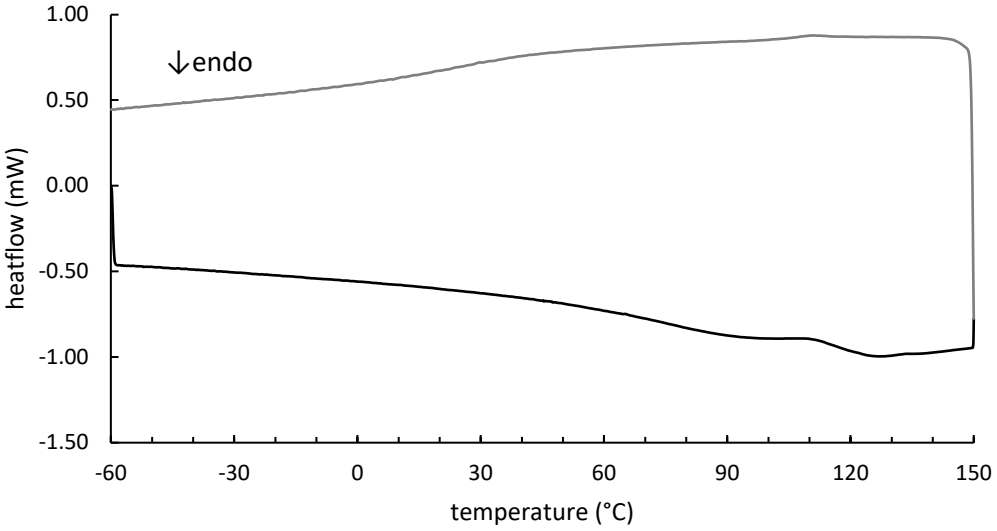

Figure S4. DSC heating (black) and cooling (gray) curves for **PS-5** from the third cycle. The third cycle was identical to the second cycle. The first cycle was obstructed by the desorption of moisture. The heating cycle exhibited a broad and convoluted T_g characteristic of cellulose from ~30–90 °C and two overlapping glass transitions with a midpoint of 120 °C. The cooling cycle showed similar transitions on cooling.

7. DSC of PS-6

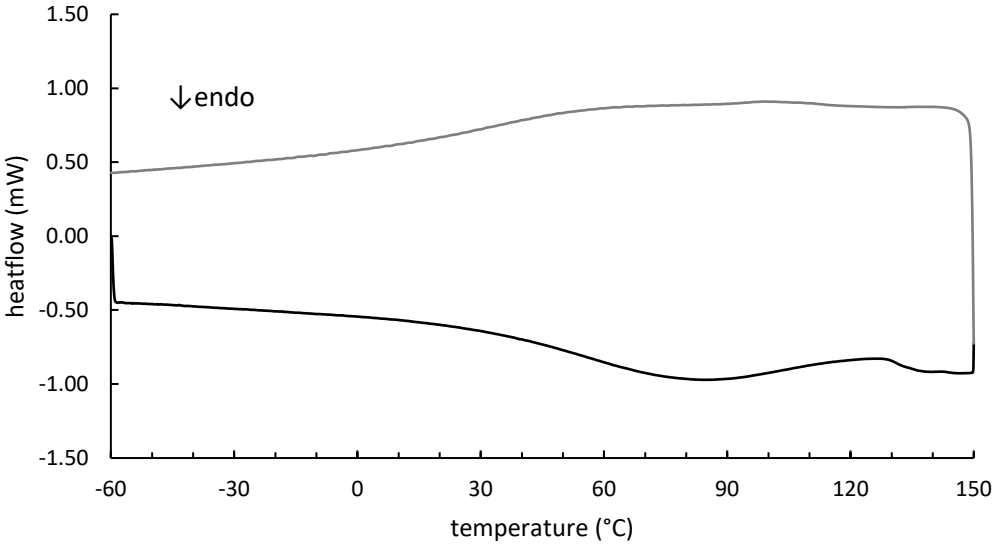

Figure S5. DSC heating (black) and cooling (gray) curves for **PS-6** from the third cycle. The third cycle was identical to the second cycle. The first cycle was obstructed by the desorption of moisture. The heating cycle exhibited a broad T_g characteristic of cellulose from ~30–90 °C and two overlapping glass transitions with a midpoint of 137 °C. The cooling cycle showed similar transitions on cooling.

8. DSC of PS-7

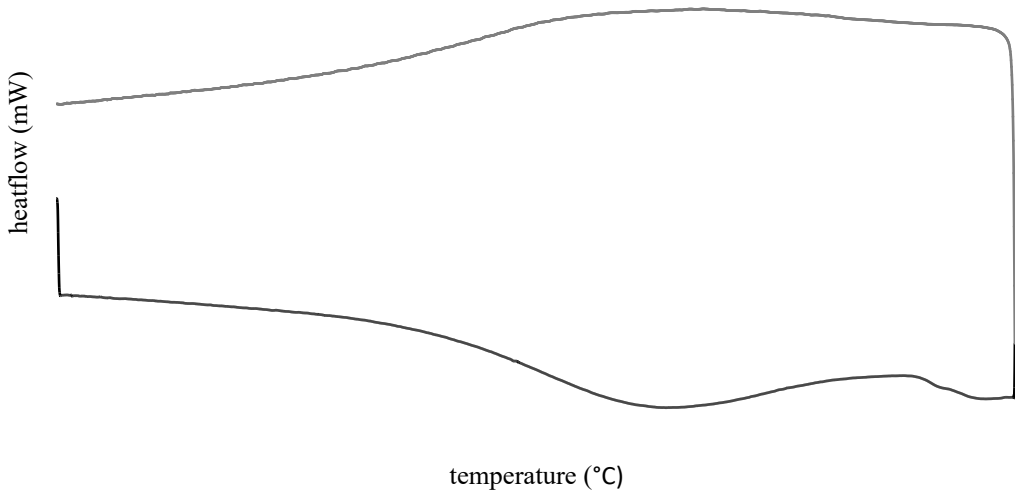

Figure S6. DSC heating (black) and cooling (gray) curves for **PS-7** from the third cycle. The third cycle was identical to the second cycle. The first cycle was obstructed by the desorption of moisture. The heating cycle exhibited a broad T_g characteristic of cellulose from ~30–90 °C and two overlapping glass transitions with a midpoint of 132 °C. The cooling cycle showed similar transitions on cooling.

9. DSC of PS-8

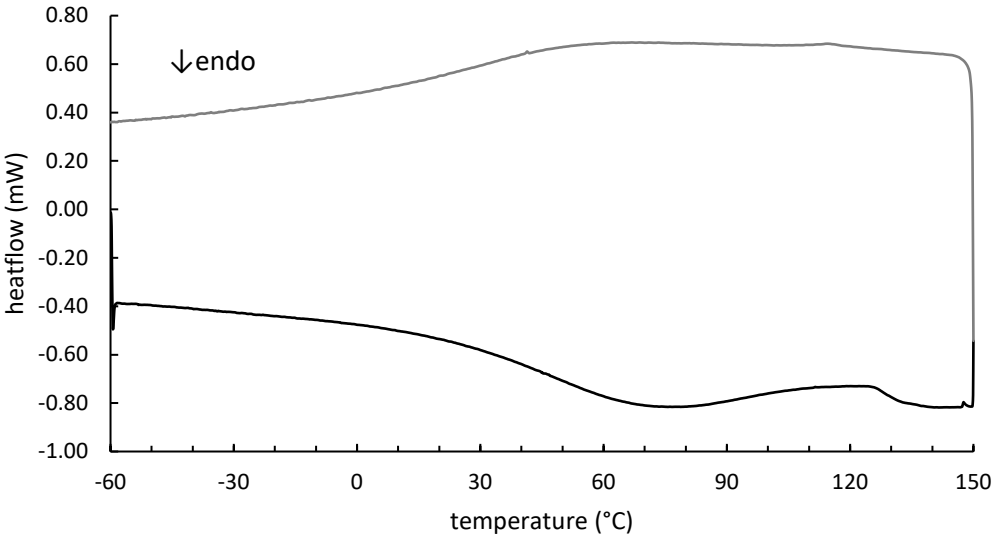

Figure S7. DSC heating (black) and cooling (gray) curves for **PS-7** from the third cycle. The third cycle was identical to the second cycle. The first cycle was obstructed by the desorption of moisture. The heating cycle exhibited a broad T_g characteristic of cellulose from ~30–90 °C and two overlapping glass transitions with a midpoint of 129 °C. The cooling cycle showed similar transitions on cooling.

10. DSC of unfractionated peanut shells

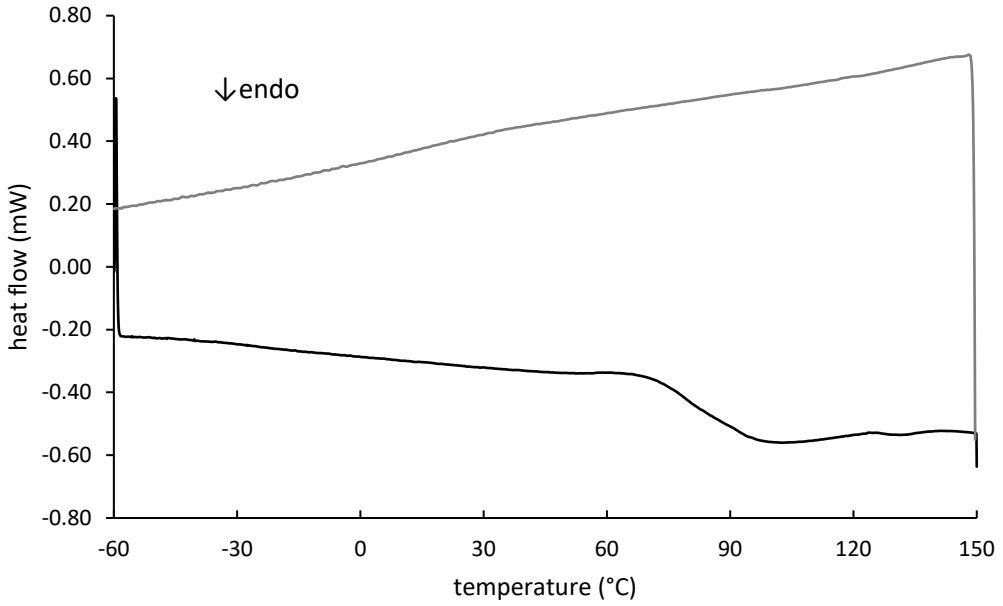

Figure S8. DSC heating (black) and cooling (gray) curves for unfractionated peanut shells from the third cycle. The third cycle was identical to the second cycle. The first cycle was obstructed by the desorption of moisture. The heating cycle exhibited a pronounced and narrower T_g than was seen in **PS-X** attributable to cellulose with a midpoint of 83 °C and a T_g attributable to lignin at 127 °C. The cooling cycle showed similar transitions on cooling. Unlike peanut shell fractions **PS-X**, unfractionated peanut shells produced exceptionally reproducible results upon replicate analysis.

11. IR of PS-X

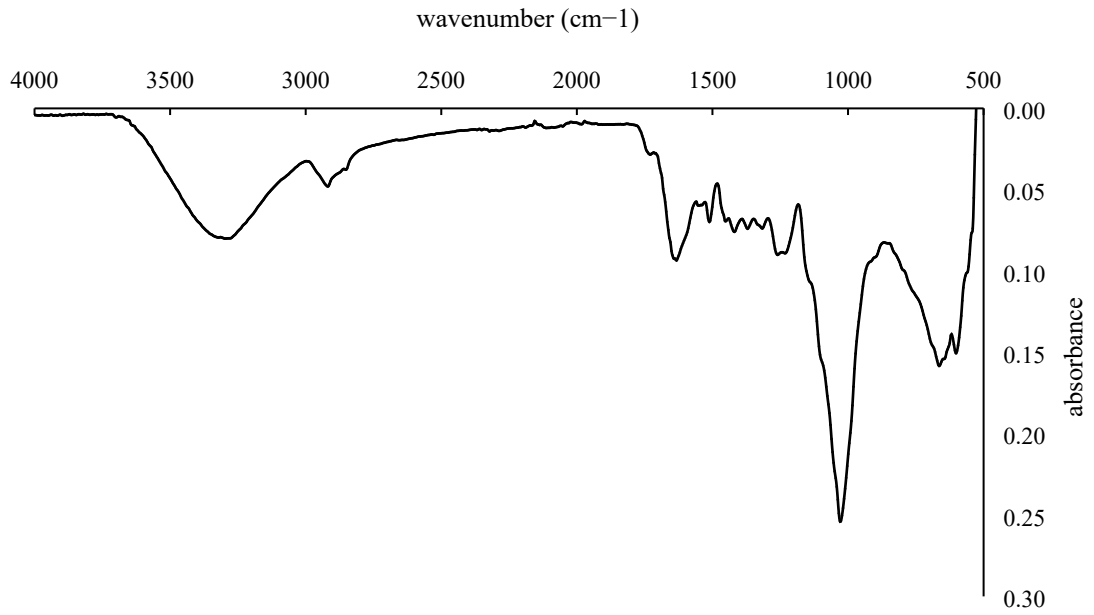

Figure S10. Representative IR spectrum of **PS-X**. All traces were nearly indistinguishable however **PS-8** was selected for presentation due to better contact with the ATR crystal providing the best resolution.

12. Digital Images of PSS-1 and PSS-2

PSS-1 PSS-2

Figure S10. Digital images of **PSS-1** and **PSS-2** upon cooling exhibiting significant phase separation.

13. TGA of PSS-X

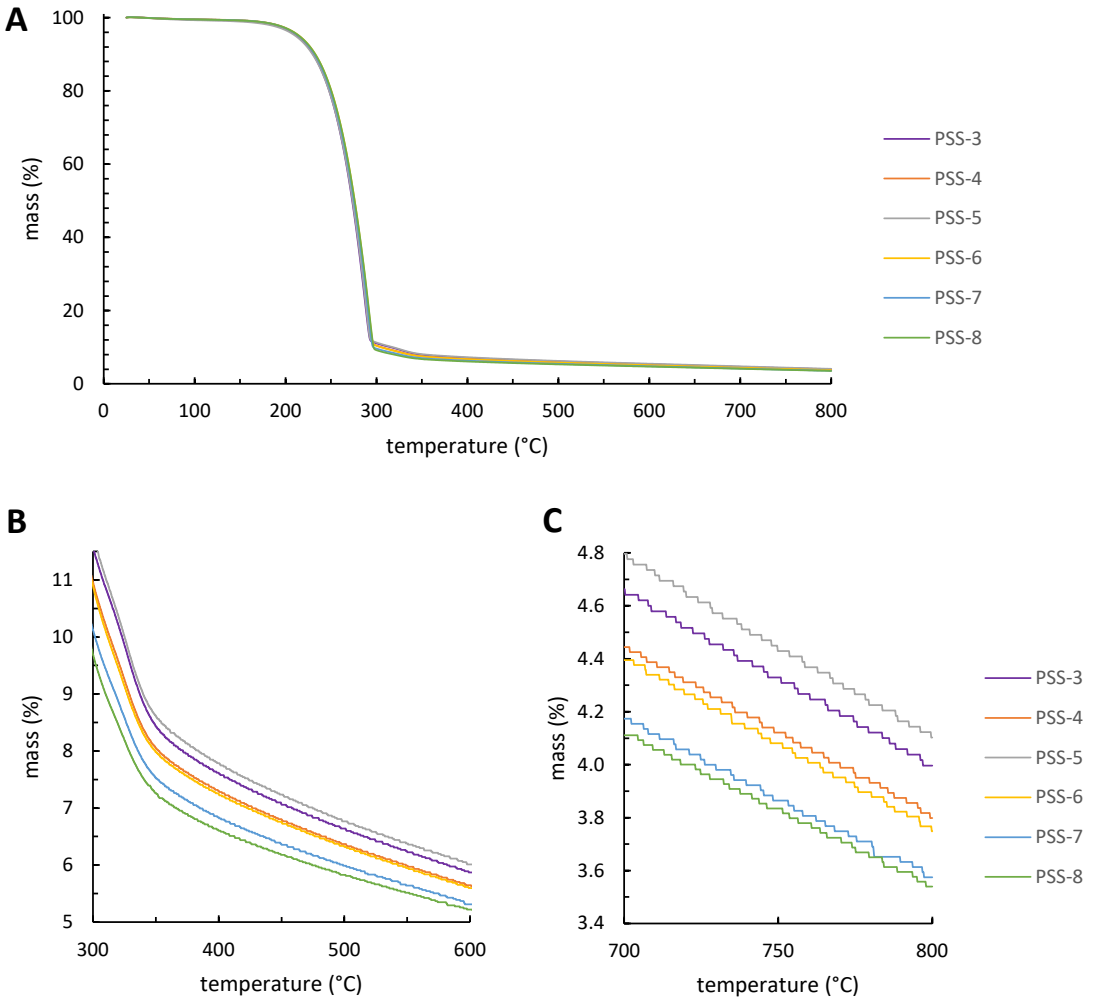

Figure S11. TGA traces of **PSS-X** showing a similar trend as was seen for **PS-X** starting materials but influenced by the amount of sulfur incorporated into each material where composites containing more sulfur decomposed more completely. The curves look quite similar when presented as the full range form 25–800 °C (**A**) but show slight discrepancies during the second small mass loss attributed to the organic portion of the material (**B**) and when looking at the char yield at 800 ° (**C**).

14. DSC of PSS-3

A

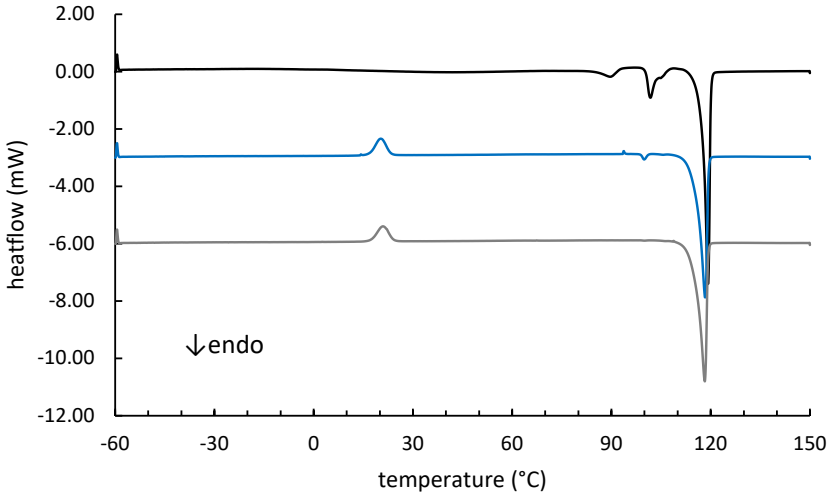

B

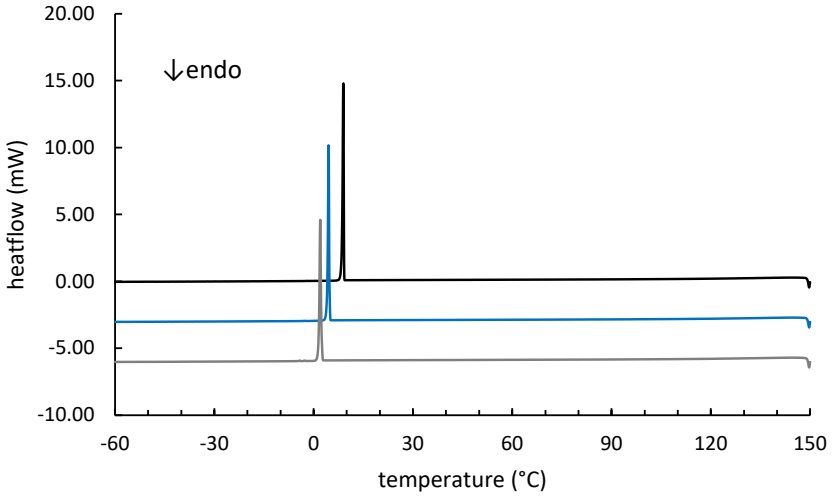

Figure S12. DSC traces for **PSS-3** showing heating cycles 1–3 (**A**) and cooling cycles 1–3 (**B**) with the first cycle in black, the second cycle in blue, and the third cycle in gray. Each sequential trace is offset by 3 mW for visual clarity. The first heat shows endotherms with local maxima at 89.7, 101.7, and 119.0 °C. The second heat shows an exotherm at 20.3, a small endotherm at 99.9, and another endotherm at 118.2 °C. The third heat shows an exotherm at 20.9 and an endotherm at 118.1 °C. The cooling cycles show crystallization exotherms at 9.3, 4.8, and 2.2 °C for the first, second, and third cooling cycles, respectively.

15. DSC of PSS-4

A

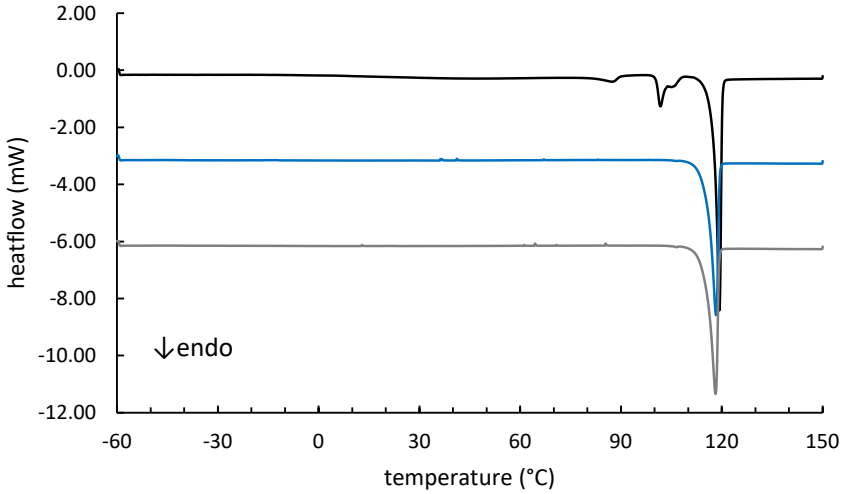

B

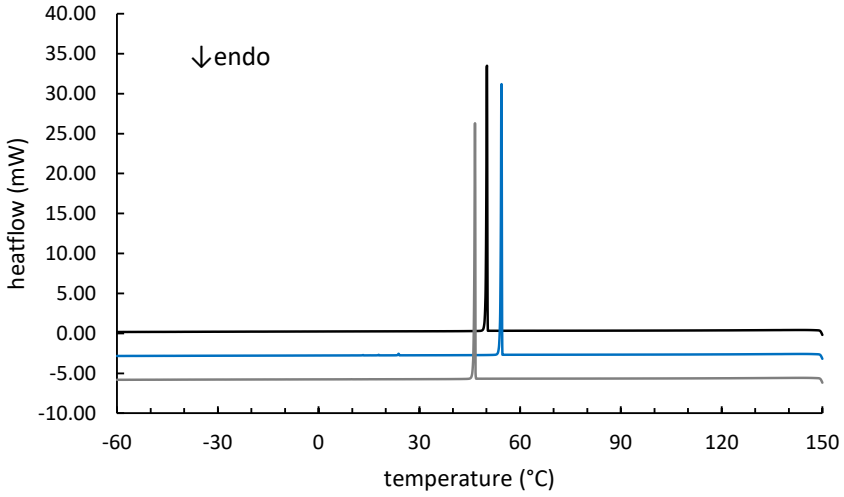

Figure S13. DSC traces for **PSS-4** showing heating cycles 1–3 (**A**) and cooling cycles 1–3 (**B**) with the first cycle in black, the second cycle in blue, and the third cycle in gray. Each sequential trace is offset by 3 mW for visual clarity. The first heat shows endotherms with local maxima at 87.4, 101.7, and 118.9 °C. The second heat shows a single endotherm at 118.0 °C. The third heat shows a single endotherm at 117.9 °C. The cooling cycles show crystallization exotherms at 51.1, 55.5, and 47.5 °C for the first, second, and third cooling cycles, respectively.

16. DSC of PSS-5

A

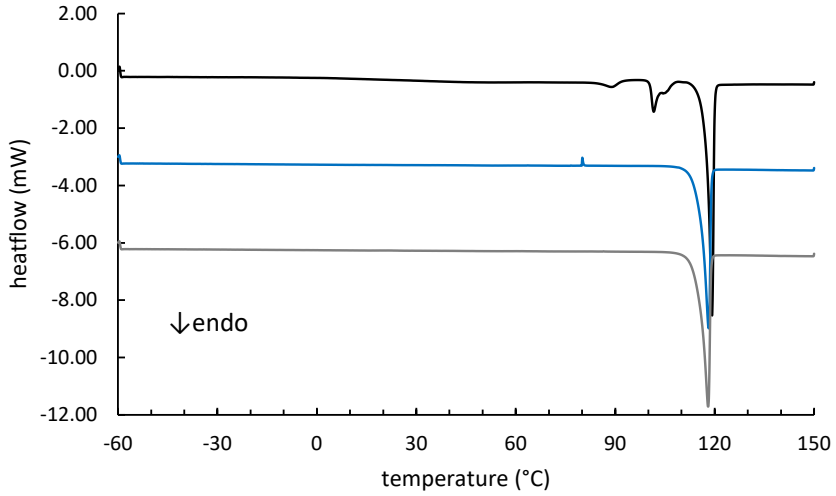

B

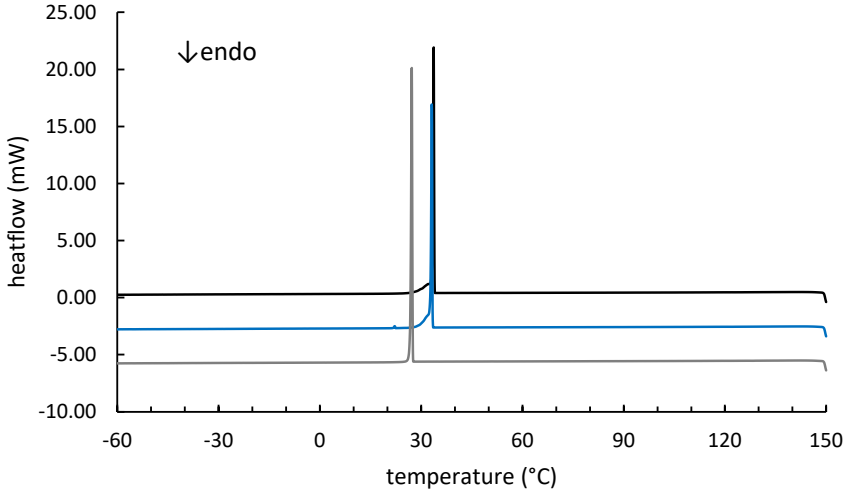

Figure S14. DSC traces for **PSS-5** showing heating cycles 1–3 (**A**) and cooling cycles 1–3 (**B**) with the first cycle in black, the second cycle in blue, and the third cycle in gray. Each sequential trace is offset by 3 mW for visual clarity. The first heat shows endotherms with local maxima at 88.9, 101.5, and 118.9 °C. The second heat shows a single endotherm at 117.9 °C. The third heat shows a single endotherm at 117.8 °C. The cooling cycles show crystallization exotherms at 34.3, 33.7, and 27.9 °C for the first, second, and third cooling cycles, respectively.

17. DSC of PSS-6

A

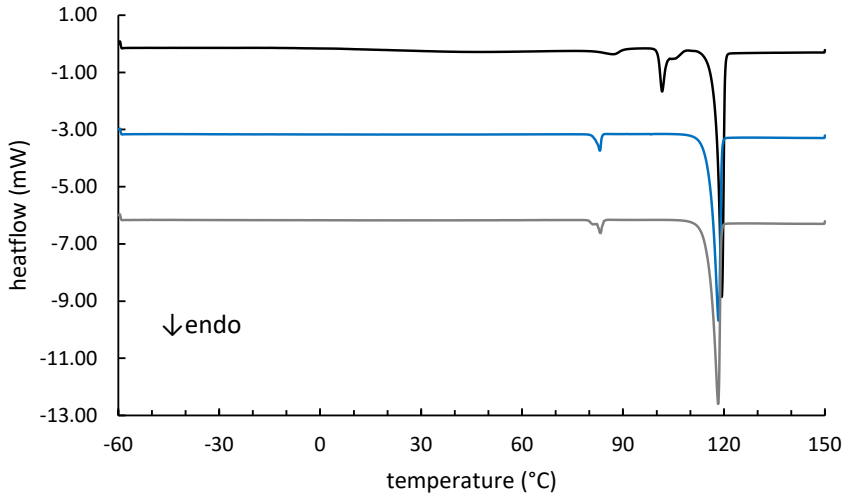

B

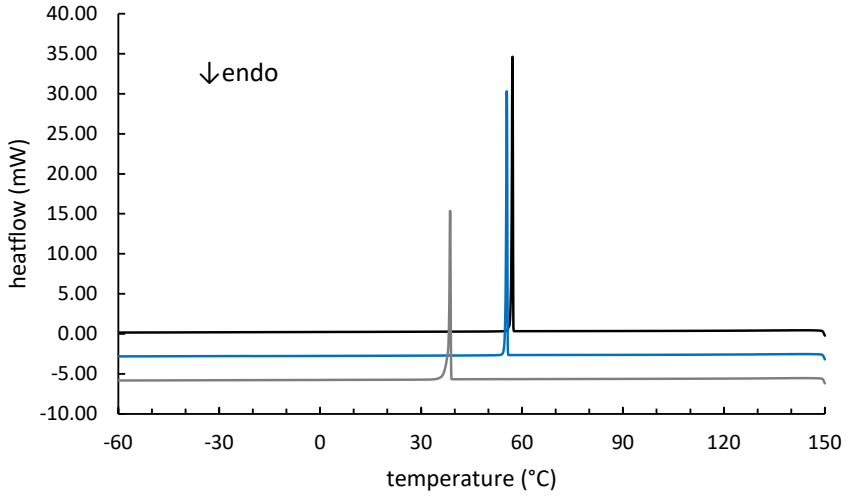

Figure S15. DSC traces for **PSS-6** showing heating cycles 1–3 (**A**) and cooling cycles 1–3 (**B**) with the first cycle in black, the second cycle in blue, and the third cycle in gray. Each sequential trace is offset by 3 mW for visual clarity. The first heat shows endotherms with local maxima at 87.2, 101.5, and 119.0 °C. The second heat shows an endotherm at 83.1 and 118.2 °C. The third heat shows an endotherm at 83.2 and 118.0 °C. The cooling cycles show crystallization exotherms at 58.2, 56.4, and 39.2 °C for the first, second, and third cooling cycles, respectively.

18. DSC of PSS-7

A

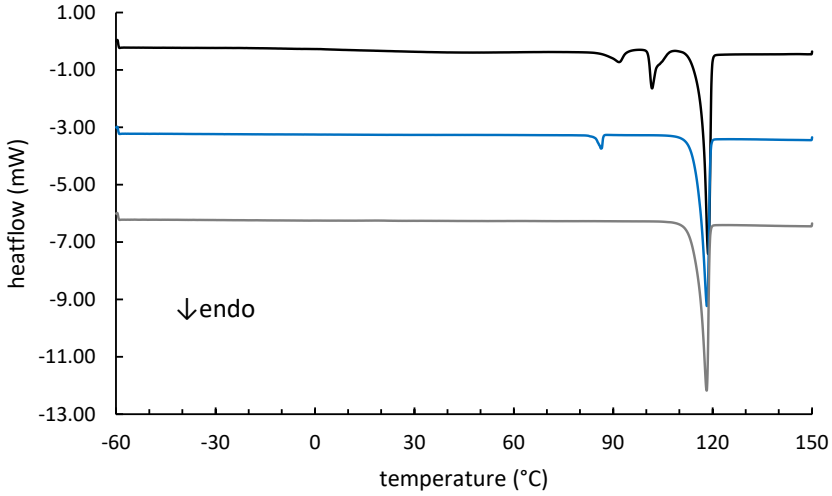

B

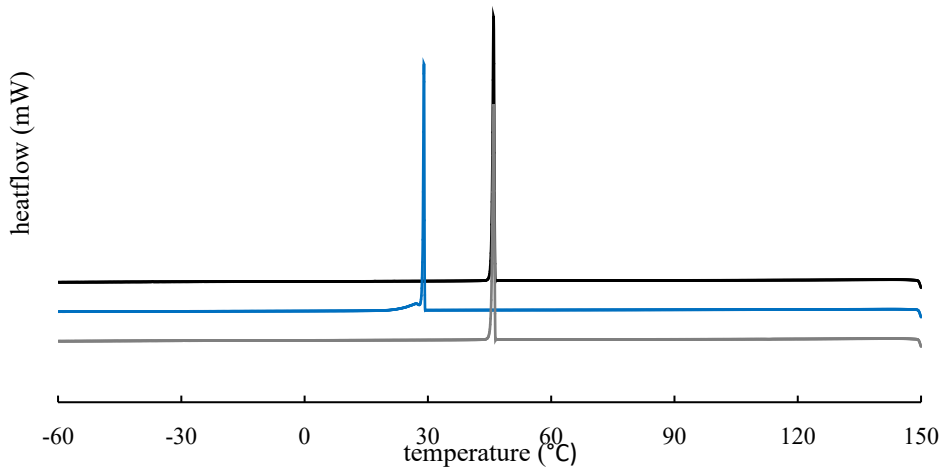

Figure S16. DSC traces for **PSS-7** showing heating cycles 1–3 (**A**) and cooling cycles 1–3 (**B**) with the first cycle in black, the second cycle in blue, and the third cycle in gray. Each sequential trace is offset by 3 mW for visual clarity. The first heat shows endotherms with local maxima at 91.7, 101.7, and 118.4 °C. The second heat shows an endotherm at 86.3 and 118.0 °C. The third heat shows a single endotherm at 117.9 °C. The cooling cycles show crystallization exotherms at 46.8, 29.6, and 46.7 °C for the first, second, and third cooling cycles, respectively.

19. DSC of PSS-8

A

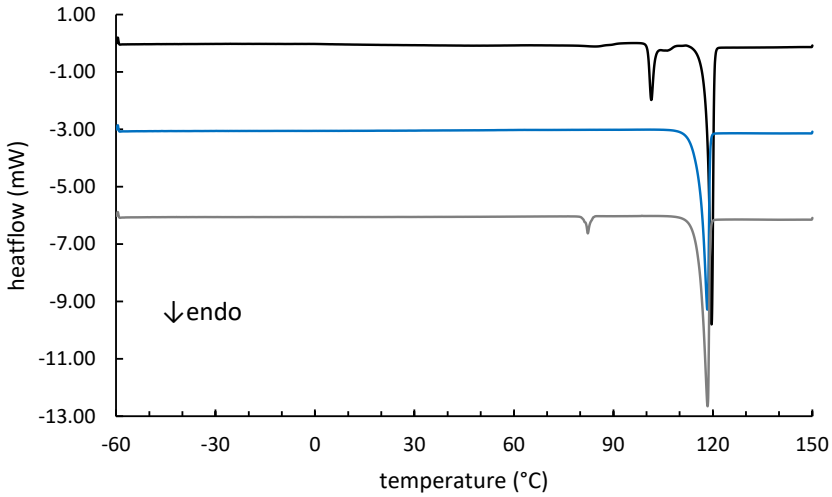

B

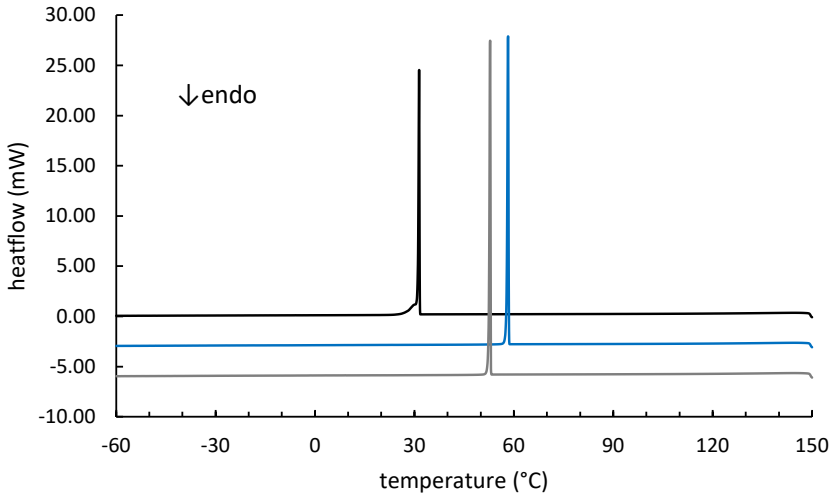

Figure S17. DSC traces for **PSS-8** showing heating cycles 1–3 (**A**) and cooling cycles 1–3 (**B**) with the first cycle in black, the second cycle in blue, and the third cycle in gray. Each sequential trace is offset by 3 mW for visual clarity. The first heat shows endotherms with local maxima at 84.9, 101.4, and 119.2 °C. The second heat shows a single endotherm at 118.1 °C. The third heat shows an endotherm at 82.2 and 118.2 °C. The cooling cycles show crystallization exotherms at 32.1, 59.2, and 53.8 °C for the first, second, and third cooling cycles, respectively.

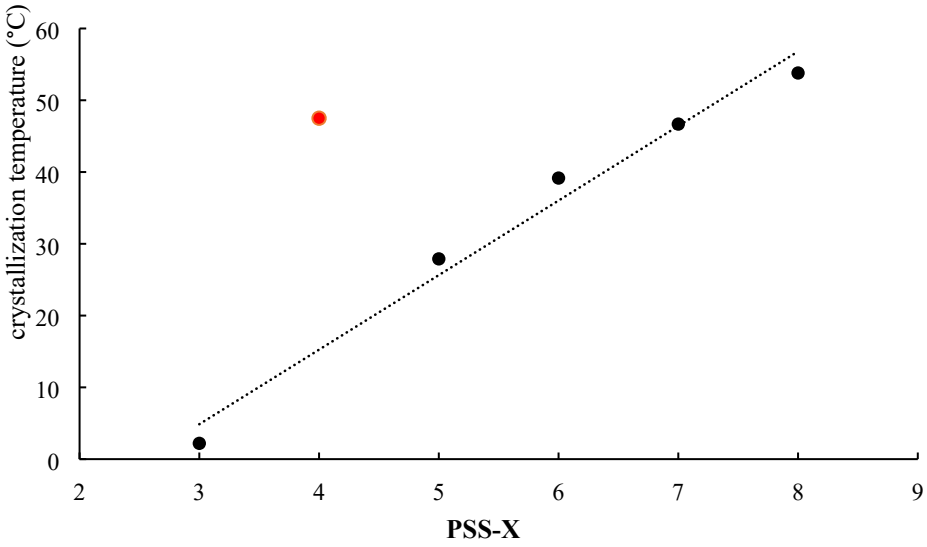

Figure S18. Plot of crystallization temperature for each **PSS-X** material taken from the third heating cycle showing a nearly linear trendline with the exception of **PSS-4** (not included in the trendline calculation). The unusually high crystallization temperature of **PSS-4** can be rationalized by the limited degree of crosslinking in the material allowing recrystallization of sulfur domains to occur more quickly upon cooling

20. DSC crystallization temperatures for PSS-X

Table S3. Crystallization temperature for **PSS-X** materials

PSS-X	crystallization temperature (°C)[a]
3	**2.2**
4	**47.5**
5	**27.9**
6	**39.16**
7	**46.68**
8	**53.8**

[a]**Taken from the third cooling cycle.**

21. ^{1}H NMR of peanut oil

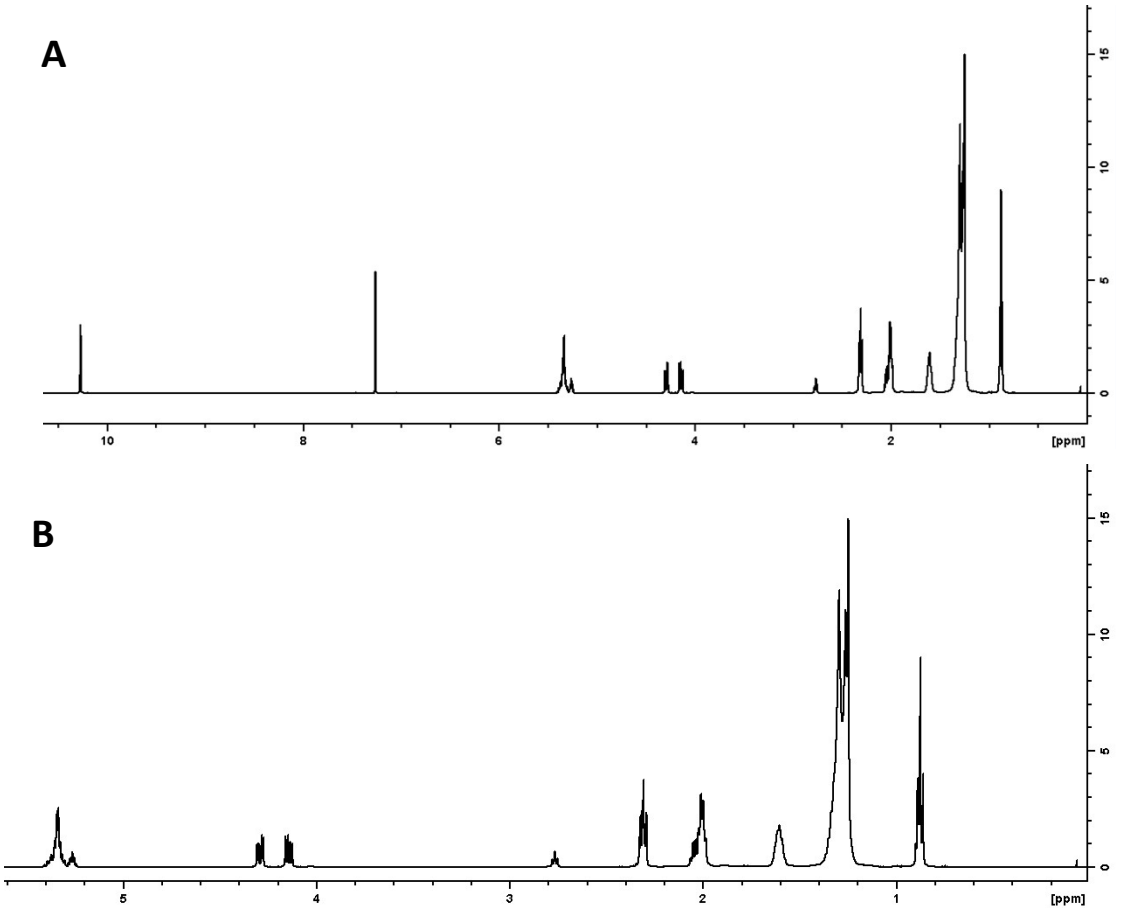

Figure S19. Proton NMR spectra of 10 mg/mL peanut oil in $CDCl_3$ (7.26 ppm) with internal standard 2,3,4,5,6-pentafluorobenzaldehyde (10.27 ppm) showing the full spectrum (**A**) and the part of the spectrum where the resonances attributable to the peanut oil are observed (**B**).

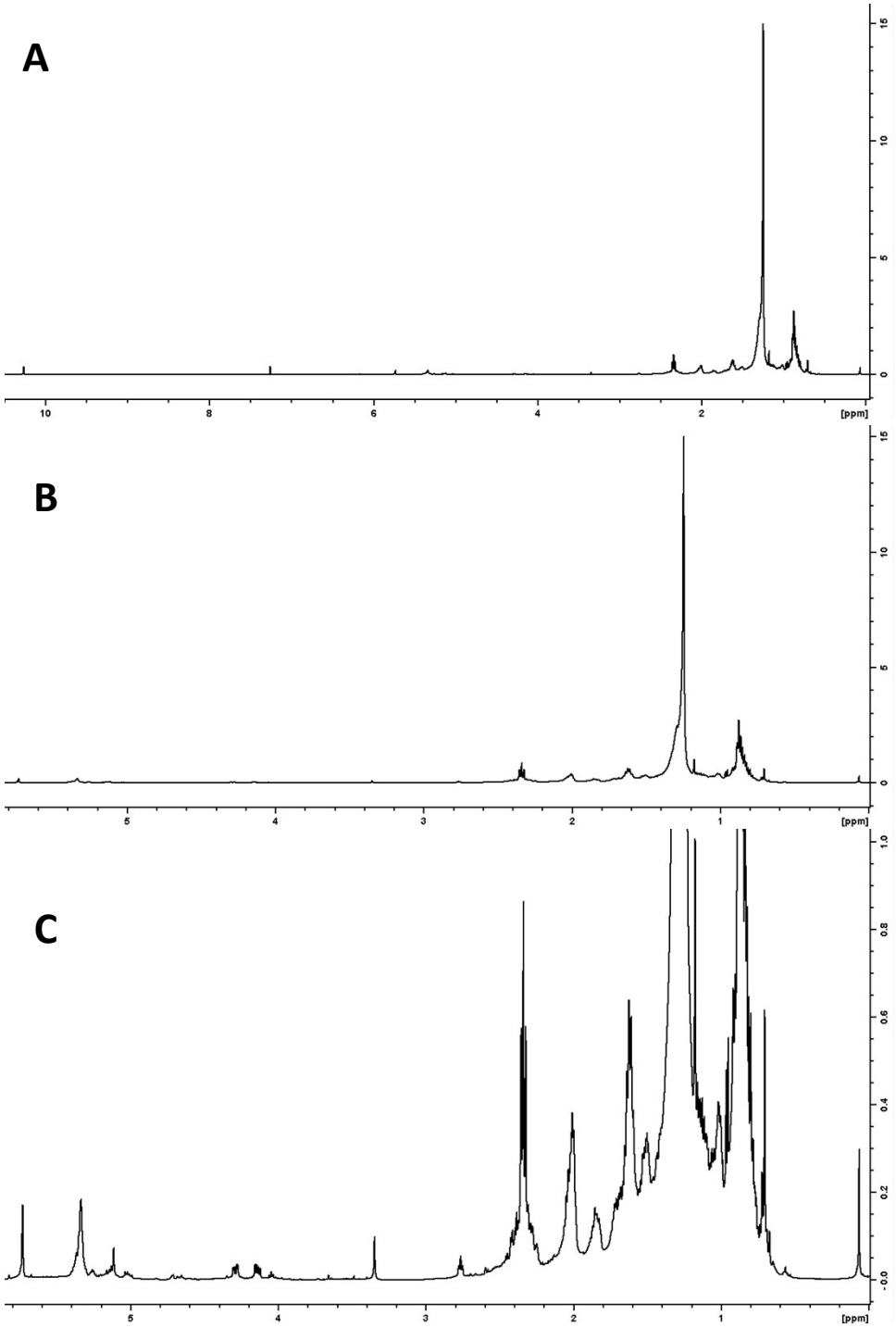

Figure S20. Proton NMR spectra of **PS-3** hexane soluble fraction in $CDCl_3$ (7.26 ppm) with internal standard 2,3,4,5,6-pentafluorobenzaldehyde (10.27 ppm) showing the full spectrum (**A**) the part of the spectrum where the resonances attributable to the peanut oil are observed (**B**), and the part of the spectrum where the resonances attributable to the peanut oil are observed with a magnified y-axis. All **PS-X** spectra looked nearly identical but with different internal standard to diagnostic peak ratios.

22. ^{1}H NMR of PS-X